Experimental and theoretical electron-scattering cross-section data for dichloromethane

K. Krupa,[1] E. Lange,[2] F. Blanco,[3] A. S. Barbosa,[4] D. F. Pastega,[4] S. d'A. Sanchez,[4] M. H. F. Bettega,[4,*] G. García,[1,*] P. Limão-Vieira,[2,*] and F. Ferreira da Silva[2]

[1]*Instituto de Física Fundamental, Consejo Superior de Investigaciones Científicas (CSIC), Serrano 113-bis, 28006 Madrid, Spain*
[2]*Laboratório de Colisões Atómicas e Moleculares, CEFITEC, Departamento de Física, Universidade NOVA de Lisboa, 2829-516 Caparica, Portugal*
[3]*Departamento de Fisica Atomica, Molecular y Nuclear, Facultad de Ciencias Fisicas, Universidad Complutense de Madrid, E-28040 Madrid, Spain*
[4]*Departamento de Física, Universidade Federal do Paraná, Caixa Postal 19044, 81531-990 Curitiba, Paraná, Brazil*

(Received 3 January 2018; published 10 April 2018)

We report on a combination of experimental and theoretical investigations into the elastic differential cross sections (DCSs) and integral cross sections for electron interactions with dichloromethane, CH_2Cl_2, in the incident electron energy over the 7.0–30 eV range. Elastic electron-scattering cross-section calculations have been performed within the framework of the Schwinger multichannel method implemented with pseudopotentials (SMCPP), and the independent-atom model with screening-corrected additivity rule including interference-effects correction (IAM-SCAR+I). The present elastic DCSs have been found to agree reasonably well with the results of IAM-SCAR+I calculations above 20 eV and also with the SMC calculations below 30 eV. Although some discrepancies were found for 7 eV, the agreement between the two theoretical methodologies is remarkable as the electron-impact energy increases. Calculated elastic DCSs are also reported up to 10000 eV for scattering angles from 0° to 180° together with total cross section within the IAM-SCAR+I framework.

DOI: 10.1103/PhysRevA.97.042702

I. INTRODUCTION

Halogen-containing molecules were identified long ago as atmospherically relevant due to long lifetimes in the Earth's troposphere and their role in the stratosphere local chemistry [1,2]. In the particular case of halogenated methanes (e.g., CH_2X_2; X = F, Cl, Br, I), once in the atmosphere either by natural or anthropogenic emissions, their main sink mechanisms are thermal decomposition, reactions with radicals, and even ultraviolet photolysis yielding halogenated methyl radicals. Although the abundance of dihalomethanes may be small, stratospheric chlorine loading can be of particular relevance if these compounds' concentrations were to increase [3]. Dichloromethane, CH_2Cl_2, used as a solvent is a volatile organic compound (VOC) with recent efforts made to investigate its remediation mechanism through a packed-bed plasma reactor [4]. This process presents several advantages for air-pollution control in detriment to other traditional VOC removal methods such as with thermal oxidation, catalytic oxidation, and adsorption [4]. In these plasma environments, processes are initiated by electron chemical reactions and so comprehensive knowledge of the dichloromethane electronic structure is relevant to establish innovative and more efficient technologies to promote or eliminate a particular chemical pathway. This certainly further improves our understanding of the sources and sinks with potential environmental implications. Electron-impact studies with dichloromethane have focused on electron attachment (rates) and resonances [5–12]. Absolute total electron-impact ionization cross sections have been obtained by Harland and co-workers [13,14] and, more recently, by Naghma *et al.* [15] from threshold up to 5000 eV through a semiempirical complex scattering potential method. Other experimental and theoretical studies include transmission-beam total-scattering cross-section measurements [16] as well as spherical complex optical potential calculations [17], differential elastic (at 20 eV only), and momentum-transfer cross sections using the Schwinger multichannel method [18].

In the present contribution, we report a combined experimental and theoretical study on the elastic differential cross sections (DCSs) from 7.0 to 30 eV. Intermediate- to low-energy electron-impact DCSs are obtained using two different theoretical methodologies, i.e., the Schwinger multichannel method implemented with pseudopotentials (SMCPP) and the independent-atom model with screening-corrected additivity rule plus interference (IAM-SCAR+I). As far as the authors are aware and given the relevance of dichloromethane in industrial applications, other experimental DCS data to compare with are scarce. This study is complemented by electron-scattering theoretical data on total, integral inelastic, electronic excitation, and ionization cross sections and compared to the available data in the literature.

The outline of our paper is as follows. In Sec. II, we briefly describe the details of our experimental procedure, and in Sec. III the theoretical calculations, with our results being presented and discussed in Sec. IV. Finally, in Sec. V, some conclusions from this work are summarized.

*Corresponding authors: bettega@fisica.ufpr.br; g.garcia@csic.es; plimaovieira@fct.unl.pt

II. EXPERIMENTAL SETUP

Elastic differential cross sections (DCSs) were obtained in a high-resolution electron energy-loss spectrometer (HREELS), VG-SEELS 400, which has been described in detailed in Ref. [19]. Briefly, a monochromatic electron beam generated with a hemispherical electron monochromator is made to cross at right angles with an effusive molecular beam target that reaches the interaction region through a 0.95-mm–inner-diameter hypodermic needle. Scattered electrons from the target gas are energy analyzed with a hemispherical electron analyzer that rotates about the gas jet from 0° to +120°, with respect to the incident electron beam, and are detected by an electron multiplier. The angular acceptance is 1.25°±0.25°. The typical base pressure in the main chamber was 5.0×10^{-5} Pa and, upon dichloromethane admission, this increased to a pressure of 1.0×10^{-3} Pa. The liquid sample was supplied from Fluka with a quoted purity of $\geqslant$99.9%. The sample was degassed by repeated freeze-pump-thaw cycles prior to use.

The energy resolution of the incident electron beam was ∼120 meV [full width at half maximum (FWHM)], with incident electron currents of a few nA (depending on the initial electron energy). For such an energy-resolution value, there could be contributions to the elastic signal from some of the lower-lying vibrational modes of CH_2Cl_2. Notwithstanding, for electron-impact energies above 10 eV, these possible vibrational contributions are expected to be very small compared to the elastic signal, and thus are not expected to make any significant contribution to the measured elastic cross sections. However, for electron-impact energies below 10 eV, special care was taken to carefully extract the elastic contribution by deconvoluting the energy-loss spectra with the Gaussian profiles. The incident electron energy was calibrated to the elastic peak. Here the absolute scale of the elastic DCS is obtained through an independent-atom model with screening-corrected additivity rule calculation with an interference-term correction (see Sec. III).

III. COMPUTATIONAL METHODS

The experimental DCSs have been interpreted with the aid of two complementary theoretical methodologies that permit one to establish the angular behavior of scattered electrons from molecules in a wide range of electron-impact energies from low to intermediate energy ($\leqslant$30 eV) and from intermediate to high energy ($\geqslant$20 eV). These are based on the well-established Schwinger multichannel method (SMC) and on a corrected form of the independent-atom model (IAM) known as the screening-corrected additivity rule (SCAR), which are briefly presented below. Such a joint experimental and theoretical procedure has been implemented recently in our laboratory in the case of electron scattering from acetone [20] and chlorobenzene [21], and revealed to be very reliable when compared to other available data in the literature. Therefore, we are confident that the procedure implemented here for dichloromethane differential cross sections can be relied upon across the studied energy range (7.0–30 eV).

A. Schwinger multichannel (SMC) method

To compute the differential and integral elastic cross sections of dichloromethane, we employed the SMC method [22,23] implemented with pseudopotentials (SMCPP) [24]. The SMC method and its implementations were recently reviewed in detail [25]; therefore, we will only discuss the theoretical aspects related to the present calculations. Our calculations were carried out in the C_{2v} symmetry group employing the experimental molecular geometry [26]. The pseudopotentials of Bachelet *et al.* [27] were used to replace the core electrons of the carbon and oxygen atoms, whereas the valence electrons are represented by six s-type, five p-type, and two d-type Cartesian Gaussian functions, generated according to Ref. [28]. For the hydrogens, we employed the $4s/3s$ basis set of Dunning [29] augmented with one p-type function with exponent 0.75. In order to avoid linear dependency in the basis set, the symmetric combinations of the d-type orbital were excluded. The scattering cross sections were computed in the static-exchange plus polarization (SEP) approximation, where the configuration state functions (CSFs) are built from products of target states with a single-particle wave function. In the simplest approximation, in which the polarization effects of the electronic cloud are neglected [known as the static-exchange (SE) approximation], the CSFs are given by a direct product between the target ground state, which is described in the Hartree-Fock level, and a single-particle function. In the SEP approximation, the direct space is augmented by considering direct products of N-electron states, obtained by performing single (virtual) excitations of the target from the occupied (hole) orbitals to a set of unoccupied (particle) orbitals, and a single-particle function to represent the scattered electron. We used the modified virtual orbitals (MVOs) [30], as generated in the field of the cation with charge +6, to represent the particle and scattering orbitals. All the valence orbitals were employed as hole orbitals and the first 48 MVOs were used as particle and scattering orbitals, resulting in 23 135 CSFs, when singlet- and tripled-coupled excitations were employed. In order to check the stability of our calculations and the influence of triplet-coupled excitations, we also performed two extra calculations: the first one also employed the first 48 MVOs as particle and scattering orbitals but employed only singlet-coupled excitations, whereas the second extra calculation (only for the resonant symmetries A_1 and B_2) employed the 68 first MVOs, also considering only singlet-coupled excitations. Table I summarizes the number of CSFs for the three calculations performed with the SMCPP method.

Finally, we employed the standard Born-closure procedure [31] to account for scattering of higher partial waves due to the long-range character of the dipole potential. Our computed value for the dipole moment was 1.91 D, which is about 19% larger than the experimental value of 1.60 D [26].

TABLE I. Number of CSFs employed in the calculations performed with the SMCPP method.

	A_1	B_2	B_1	A_2
SEP (S+T) – 48 MVOs	6172	6061	5505	5397
SEP (S) - 48 MVOs	3201	3116	2810	2728
SEP (S) – 68 MVOs	6232	6115		

B. Independent-atom model (IAM)

Full details of the independent-atom model with screening-corrected additivity rule calculation [32,33] have been presented on several occasions, whereas with an interference-term correction (IAM-SCAR + I) [34], it has been recently used within the context of electron scattering from *para*-benzoquinone [35]. Briefly, Blanco and García [34] have shown that even at high electron-impact (and positron-impact) energies, multiple scattering effects are not negligible and the interference terms can appreciably modify both the differential and integral calculated cross sections. Their modification and correction to the original additivity rule in the IAM-SCAR method [32,33] by including the contribution of such terms has been validated [34] by further solving the three-dimensional Lippmann-Schwinger equation for multicenter potentials using a procedure established by Polasek *et al.* [36]. This method has improved the former IAM-SCAR to produce reliable elastic scattering differential cross sections to within 10% of the experimental data at energies greater than 30 eV, and even at impact energies above 10–20 eV in some molecular targets (see, e.g., Ref. [37] for phenol molecule). We are unaware of other experimental or theoretical DCS data for dichloromethane that is currently available at this impact energy. As so, we make use of IAM-SCAR+I to obtain the qualitative behavior of the experimental elastic scattering DCS data to within 10%. Additional differential rotational cross sections are calculated by considering dipole interactions within the framework of the Born approximation.

IV. RESULTS AND DISCUSSION

In this section, we present a comprehensive discussion of the experimental and theoretical elastic differential cross sections, showing the strong agreement between experiment and theory as well as total (including rotational), integral inelastic, electronic excitation, and ionization cross sections. The results are compared with previous data available in the literature whenever possible. Dichloromethane, CH_2Cl_2, is a polar molecule with appreciable permanent dipole moment (1.60 D) and molecular polarizability (α) of considerable magnitude, 6.656 $Å^3$ [26], and we can anticipate that this is expected to play a key role in determining the magnitude and the angular and energy-dependent behavior of the low- to intermediate-energy electron-scattering cross sections.

A. Differential cross sections (DCSs)

The measured electron-scattering elastic differential cross sections (DCSs) are presented in Fig. 1 at four different impact energies, from 7.0 to 30 eV for scattering angles from 8° to 120°, together with the corresponding theoretical results from the application of the SMCPP and IAM-SCAR+I models. To our knowledge, there is only one theoretical elastic differential cross section (DCS) for the CH_2Cl_2 molecule, by Natalense *et al.* [18], at impact energy of 20 eV; however, there are no elastic DCSs for the dichloromethane in the low-energy range covered in the present work, i.e., below 20 eV. The experimental absolute values have been derived from the theoretical methods, from which the data have been rescaled at 30° scattering angle for 7, 10, and 20 eV from SMCPP and for 30 eV from IAM-SCAR+I. The experimental DCSs are tabulated as numerical values in Table II. A close inspection of Fig. 1 shows that the cross sections are enhanced in the forward-scattering angles. Such behavior is not surprising since at those very small scattering angles the cross section is dipole driven. Moreover, the considerable high value of the polarizability also reflects the magnitude and the angular and energy-dependent behavior of the low- to intermediate-energy electron-scattering cross sections. Special attention must be taken to the data points at 8°–10° scattering angles, in particular at low electron-impact energies, where the experimental points overestimate the theoretical data which may be due to angular resolution limitation (<2°). Nonetheless, the qualitative behavior of these experimental data points agrees with the dipole moment and polarizability-dependent cross section of CH_2Cl_2.

Experimental elastic DCSs are compared in this figure with the theoretical SMCPP and IAM-SCAR+I calculations. The Schwinger multichannel method implemented with pseudopotentials agrees very well up to 20 eV and overestimates the experimental data for 30 eV. This is due to the approximation employed in the present calculation that does not account for relevant inelastic processes, such as electronic excitation and ionization, which are already operative at those energies. Hence, one would expect a lowering of the elastic cross section towards the experimental data since opening those channels would allow flux loss from the elastic to the inelastic channels. This has been clearly identified recently; for further details, see Refs. [37,38] and references therein. As far as the IAM-SCAR+I method is concerned, a better agreement with the experimental DCS is observed for electron-impact energies above 20 eV. Another relevant aspect of Fig. 1 is that we also include in the IAM-SCAR+I the contribution of the calculated differential rotational cross sections, indicated as IAM-SCAR+I+Rot. We clearly observe that in the forward direction, the differential and rotational summed cross section is in excellent agreement with the SMCPP method. This is another assertion of the validation of both methods in the description of the rotationally summed elastic differential cross-section angular dependence at particularly low-scattering angles. From the point of view of the shape of the differential cross sections, at 30 eV two discernible minima at 70° and 140° are visible, where the latter becomes shallower at 20 eV and disappears below 10 eV and the former shifts to lower scattering angles with decreasing electron-impact energies.

In Fig. 2, we show our calculated elastic integral cross section (ICS) obtained in the IAM-SCAR+I and SMCPP calculations. The IAM-SCAR+I ICS were obtained by adding to these ICS values the rotational excitation integral cross sections. Experimental values determined from integration of the DCSs are also included for comparison. These ICSs were obtained from the measured DCSs extrapolated for scattering angles $\theta > 120°$ by using the theoretical angular distributions of the present IAM-SCAR+I calculations above 20 eV and the SMCPP theoretical results below 10 eV, whereas for scattering angles $\theta \leqslant 10°$, extrapolation was performed with the aid of the IAM-SCAR+I+Rot. Of relevance is that the inclusion of the rotational contribution in the IAM-SCAR+I method results in an excellent agreement with the SMCPP at low-scattering angles and even at low-impact energies. A detailed inspection of Fig. 2 also shows that both theoretical methods, i.e., IAM-SCAR+I

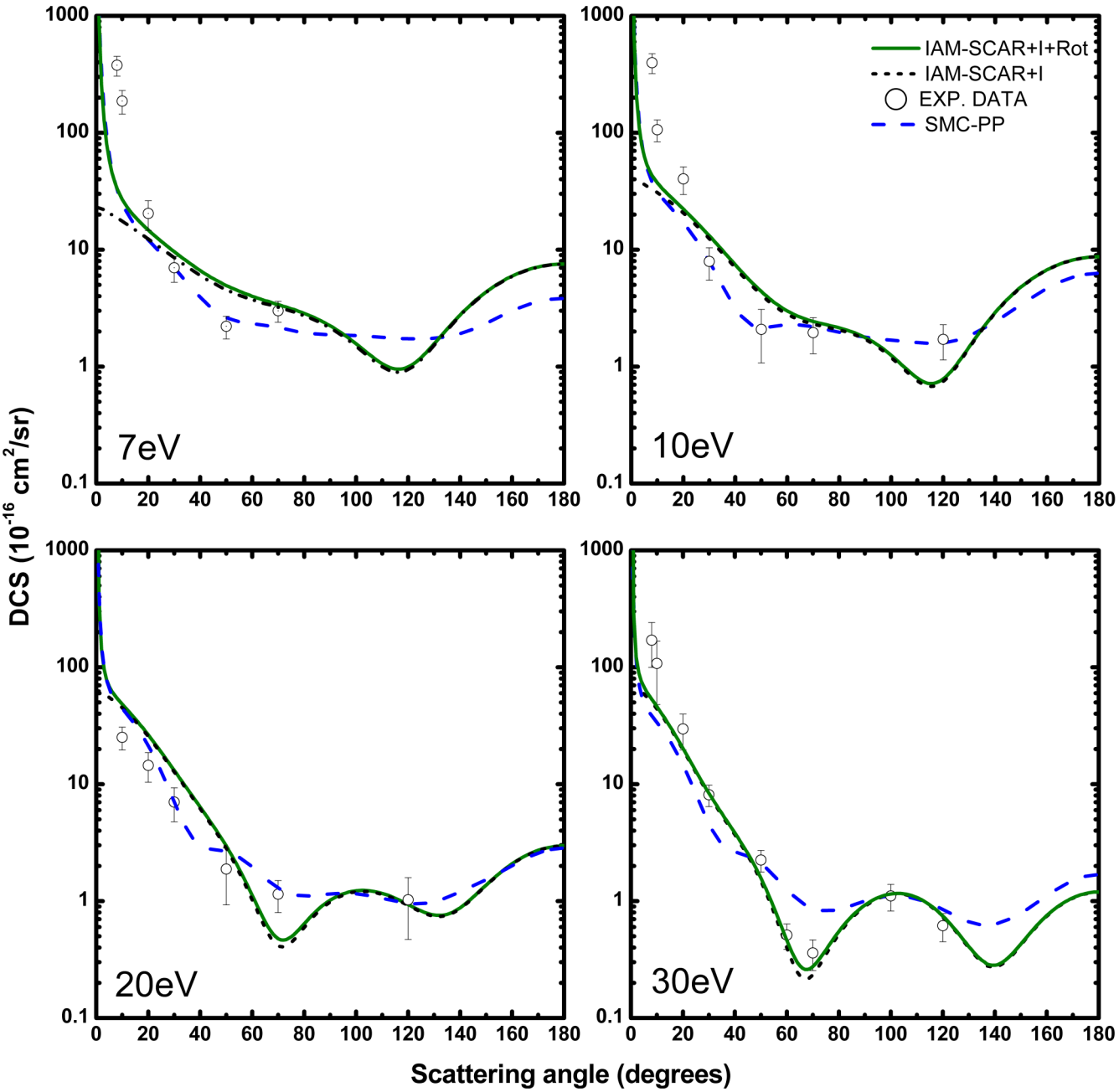

FIG. 1. Present DCS (10^{-16} cm^2/sr) for elastic electron scattering from CH_2Cl_2 in the incident electron energy region 7.0–50 eV. (•) present elastic DCS. Solid curves: Our SMCPP and IAM-SCAR+I calculations.

elastic and SMCPP, still show some discrepancies as to the magnitude of the cross sections, although compared with the experiment the shape of the cross section is in good accord. However, we notice that the SMCPP method seems to be in better agreement with the experimental data magnitude.

B. Elastic cross section at low energies

A detailed analysis of the SMCPP ICS reveals the presence of at least three resonances. There is one resonance at 0.5 eV that is due to an A_1 symmetry, one at 2.3 eV that comes from the B_2 symmetry, and a huge bump at around 10 eV. This bump comes actually from the overlap of three resonant states: one from the B_1 symmetry around 7.0 eV (in good agreement with Scheunemann and co-workers [10]), one from the A_1 symmetry, and one from the A_2 symmetry, both at around 10 eV. We estimated the width of the two low-lying resonances by fitting the resonant structure to a Breit-Wigner profile and obtained values of 0.44 and 0.71 eV. Regarding the position of the resonances, the calculated cross section places the low-lying A_1 resonance at around 0.5 eV, which is lower than the value of 0.8 eV related to the negative-ion yield from [10] and the value from electron transmission spectroscopy (ETS) of 1.2 eV [39]. We attribute this small discrepancy between theory and experiment to a possible overcorrelation of the resonance due to the polarization scheme employed in the calculation. In the SMC method, the target state is not correlated and if

TABLE II. Experimental differential (10^{-16} cm^2 sr^{-1}) and integral cross sections (10^{-20} m^2) for elastic scattering from CH_2Cl_2. Errors on the DCSs are typically 15%–20% and for the ICS are 26%–28%.

Angle (degrees)	Impact energy			
	7.0	10.0	20.0	30.0
8	377.9	397.5	1786.6	170.6
10	186.9	106.2	25.2	107.8
20	20.4	40.3	14.5	29.7
30	7.0	7.9	7.0	8.1
50	2.2	2.08	1.9	2.2
60				0.5
70	3.0	1.9	1.2	0.4
80				1.1
120		1.7	1.03	0.6
ICS	126.6	149.1	104.2	86.2

the polarization scheme is not well balanced with the target description (Hartree-Fock level), the resonance position is lower than the experimental value. As mentioned above, in order to check the influence of the triplet-coupled excitations in the cross sections, we performed two other calculations in the SEP approximation considering only singlet-coupled excitations. In the first calculation, we used the first 48 MVOs as particle and scattering orbitals, resulting in approximately 3000 CSF in each resonant symmetry [half of the number of CSFs used in the SEP (S+T) calculation presented in Fig. 2]. In this calculation, the first σ^* resonance is located at 1.6 eV with a width of 1.41 eV and the second resonance is located at 3.8 eV with a width of 2.48 eV. For the second theoretical method, our goal was to preserve about the same number of CSFs in the SEP(S+T) calculation. We then used the first 68 MVOs as particle and scattering orbitals only for A_1 and B_2 symmetries with around 6000 CSFs in each symmetry. In Fig. 3, we present the symmetry decomposition of the integral cross section for the three calculations mentioned above. It is possible to observe that when we allow singlet- and triplet-coupled excitations, the first resonance is overcorrelated with respect to the experimental data [10]. On the other hand, those CSFs are important to correctly describe the position of the second resonance. Our calculation shows that using only singlet coupling, the resonance positions converge to 1.5 eV for the first and 3.6 eV for the second, even if the number of CSF is augmented. Table III summarizes the calculated resonance positions obtained with each calculation as well as presents a comparison with the experimental data (ETS). In Fig. 3, we show the first two empty orbitals of CH_2Cl_2 obtained from the electronic structure calculations. These orbitals represent well the molecular region accessed by the incoming electron during the resonances and, although their calculated energy is not directly related to the observed shape resonances, it is possible to relate them by using an empirical scaling relation. Employing the scaled relation from Burrow *et al.* [39] for the $\sigma^*_{C\text{-}Cl}$ resonances, the two low-lying shape resonances were estimated at 1.2 and 2.6 eV, respectively. In general, the low-lying resonance positions obtained in the calculations using only singlet-coupled excitations agree well with the ETS data and with the vertical attachment energy (VAE).

C. Total, integral inelastic, electronic excitation, and ionization cross sections

The numerical values of these cross sections are presented in Table IV. In Fig. 4, we show our calculated total, total plus rotational, integral inelastic, electronic excitation, and ionization cross sections. Some of these are also compared with the available data in the literature [15–17]. A

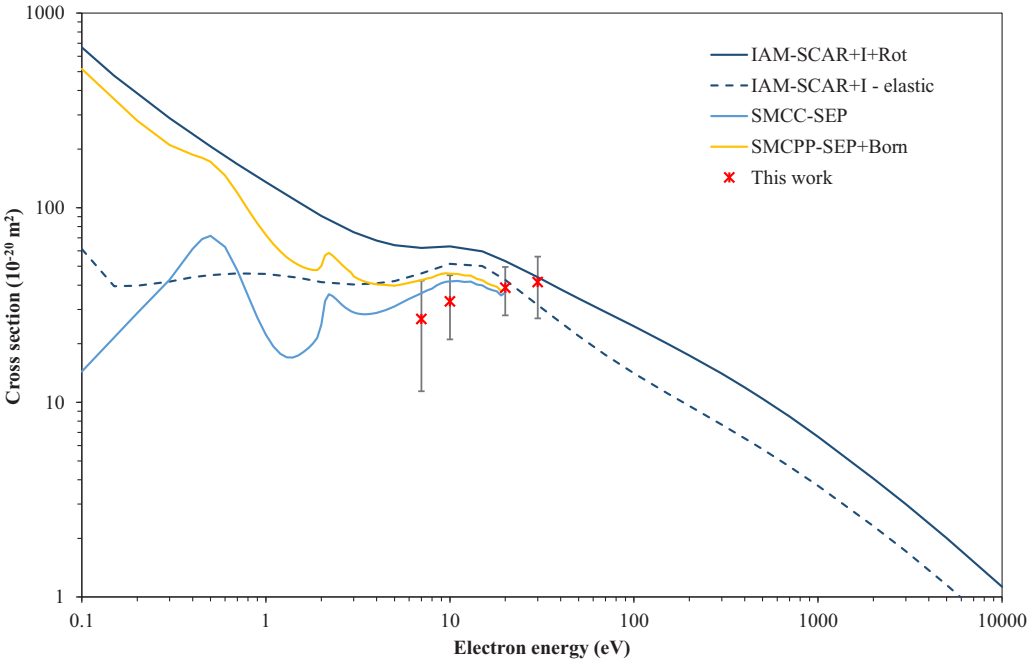

FIG. 2. Integral cross sections (10^{-20} m^2) including the experimental data on electron scattering from dichloromethane together with the theoretical calculations using the SMCCPP and the IAM-SCAR+I methods. Also included is the IAM-SCAR+I+Rot cross section.

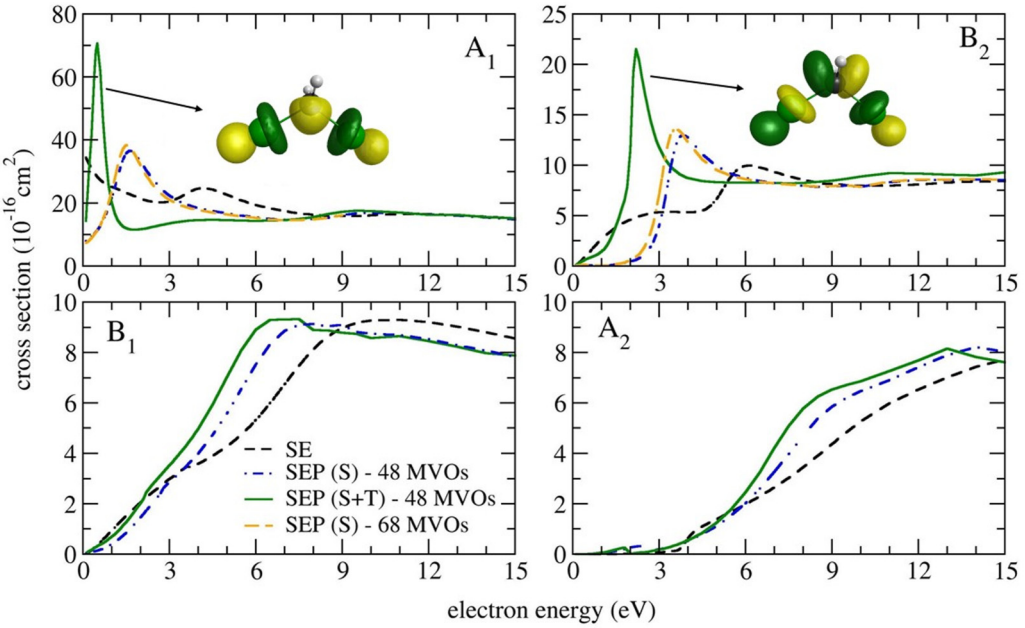

FIG. 3. Symmetry decomposition of the calculated SMCPP integral cross section (10^{-16} cm^2) of CH_2Cl_2. The insets represent the resonant molecular orbitals of σ^* nature.

qualitative discussion of the presented cross sections needs to be evaluated in two separate groups: total cross sections and integral inelastic, where we find inconsistencies that need to be properly addressed. We start by comparing the total cross section (including rotational contribution) with the data from Karwasz *et al.* [16] and Naghma *et al.* [17]. Generally speaking, the cross-sectional values in Ref. [16] are in very good accord with the data obtained from our calculation up to 1000 eV, while the values from Ref. [17] are consistently lower. Above this energy, the data of Karwasz *et al.* [16] deviates 6–17%, whereas Naghma *et al.* [17] is consistently 25% lower. The main reason for such discrepancies is due to the fact that these authors did not properly account for the elastic channel at high electron-impact energies (above 1000 eV) and small scattering angles ($\theta \approx 0°$). We now turn our attention to the ionization cross section where in Fig. 3 we note a reasonable agreement in shape between the present data and that from Ref. [15]. We have obtained, at 70 eV, a cross section value of 7.67 Å^2 compared to 9.74 Å^2 from Naghma *et al.* [15]. Also relevant is the ionization data of Bart *et al.* [13] with an experimental value of 9.4 Å^2 at 74 eV and a value of 9.9 Å^2 at 66 eV from the Deutsch-Märk

TABLE III. Comparison of the calculated resonance positions of the two low-lying shape resonances with the experimental data obtained from ETS and scaled VAE employing the scaled relation from Burrow *et al.* [39]. Results are in eV.

	$\sigma^*(A_1)$	$\sigma^*(B_2)$
SMC (S+T)-48MVOs	0.50	2.3
SMC(S)-48 MVOs	1.6	3.8
SMC(S)-68 MVOs	1.5	3.6
ETS [39]	1.2	3.38
Scaled VAE [40]	1.2	2.6

TABLE IV. Calculated electron scattering from CH_2Cl_2 total, total + rotational, excitation, ionization, and inelastic cross sections (10^{-20} m^2).

Impact energy (eV)	Total	Total + rot.	Excitation	Ionization	Inelastic
0.1	61.32	666.40			
0.15	39.48	476.00			
0.2	39.76	386.40			
0.3	41.72	288.40			
0.4	43.96	238.84			
0.5	45.08	206.64			
0.7	45.92	167.44			
1.0	45.64	135.24			
1.5	43.68	106.96			
2.0	41.44	90.72			
3.0	40.32	74.76			
4.0	40.88	67.76			
5.0	42.00	64.12			
7.0	45.92	62.16			
10	51.53	63.28	0.01		0.01
15	51.56	59.64	1.20	0.25	1.44
20	46.76	53.20	2.36	1.84	4.20
30	39.45	43.96	2.49	5.32	7.81
40	34.83	38.08	2.30	6.83	9.13
50	31.50	34.16	2.16	7.42	9.58
70	27.10	29.12	1.90	7.67	9.58
100	23.10	24.58	1.68	7.31	8.99
150	19.12	20.13	1.46	6.47	7.92
200	16.63	17.42	1.32	5.74	7.06
300	13.50	14.06	1.12	4.70	5.82
400	11.51	11.93	1.01	3.98	4.98
500	10.11	10.44	0.90	3.47	4.37
700	8.20	8.46	0.76	2.77	3.53
1000	6.50	6.66	0.62	2.16	2.78
2000	3.98	4.06	0.39	1.28	1.67
3000	2.93	3.00	0.29	0.92	1.22
5000	1.97	2.01	0.20	0.61	0.81
10000	1.11	1.13	0.12	0.34	0.46

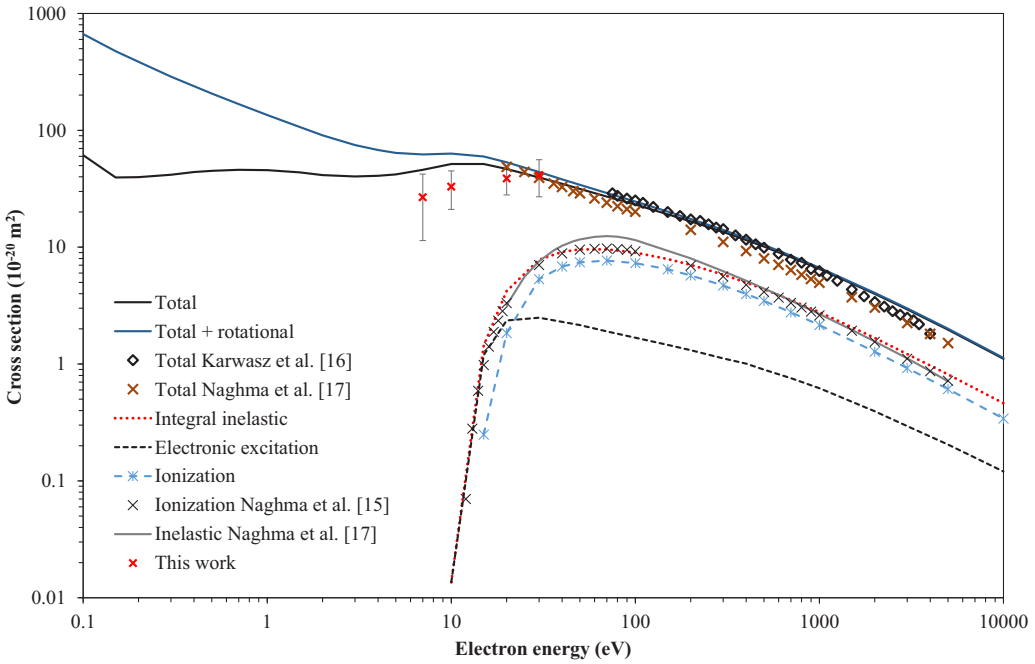

FIG. 4. Calculated electron scattering from CH_2Cl_2 total, total + rotational, excitation, ionization, and inelastic cross sections (10^{-20} m^2). Total cross sections of Karwasz *et al.* [16], Naghma *et al.* [17], ionization [15], and inelastic cross sections of Naghma *et al.* [17].

formalism. However, our cross-section maximum is ∼22% lower than Naghma *et al.* [15]. For electron-impact energies above the ionization cross-section maximum at 70 eV, the data in Ref. [15] is identical to ours within a 15% higher difference. Now we turn to a persistent misinterpretation of the underlying mechanisms that contribute to the magnitude of the integral inelastic cross section in the calculation of Naghma *et al.* [17]. This has also been made persistent in the case of electron scattering from atoms, which we have recently reported [41]. Naghma *et al.* [17] make use of a semiempirical approach to determine the ionization cross section (Q_{ion}) from the total inelastic cross section (Q_{inel}) based on the assumption that at high incident energies, $E > 500$ eV, the ratio between (Q_{ion}) / (Q_{inel}) is unity. Such rationale is built upon the condition that at those impact energies, the ionization cross section becomes predominant in the inelastic channel, while the electronic excitations rapidly decrease. Under the Born-Bethe formulation [42], at very high energies (E), the electronic excitation and ionization cross sections show similar energy dependence proportional to $[\ln(E)]/E$, meaning that the Naghma *et al.* [17] postulation is not in agreement with the first Born approximation. Therefore, these authors would have to correct their data, in particular above 500 eV where an average value of (0.82 ± 0.05) must apply rather than unity.

As a final remark, and as far as experimental investigations on the ionization and electronic excitation cross sections are concerned, we are planning a set of experiments in the Madrid laboratory to obtain comprehensive cross-sectional values to compare with those from our theoretical calculations as well as those available in the literature [13,17].

V. CONCLUSIONS

We have presented a joint experimental and theoretical investigation into the electron scattering of dichloromethane. Elastic differential cross sections were obtained and the combination of experimental electron energy-loss spectra measurements, together with two different but complementary SMCPP and IAM-SCAR+I elastic scattering differential cross-section calculations, have allowed a comprehensive description in the low to intermediate electron-impact energies of 7–30 eV. Below 20 eV, a reasonable agreement has been found between our experimental data and the SMCPP method, whereas above this energy, the IAM-SCAR+I method describes very well the experimental findings. Another interesting aspect pertains to the good accord of the IAM-SCAR+I calculation, including rotational excitations, to describe, below 20 eV, the asymptotic behavior of the DCS in the forward direction. This investigation also identified challenges in developing a strategy to perform experimental determination of the total, integral inelastic, electronic excitation, and ionization cross sections to be compared with the present calculations. Overcoming those challenges, and undertaking further energy electron scattering experiments, will form an essential part of developing complete cross-section sets for this molecular target.

ACKNOWLEDGMENTS

K.K. and F.F.S. acknowledge the Portuguese National Funding Agency FCT through Grant No. SFRH/BD/52536/2014 and Researcher Contract No. IF-FCT IF/00380/2014, and, together with P.L.V., the Research Grant No. UID/FIS/00068/2013. E.L. acknowledges the Brazilian Agency Conselho Nacional de Desenvolvimento Científico e Tecnológico (CNPq) and the Science Without Borders Programme for opportunities to study abroad. A.S.B., D.F.P., S.d'A.S. and M.H.F.B. acknowledge the Brazilian Agency Coordenação de Aperfeiçoamento de Pessoal de Nível Superior

(CAPES), under CAPES/FCT Programme (CAPES Process No. 23038.002465/2014-87, FCT Process No. 2267). S.d'A.S. and M.H.F.B. also acknowledge support from CNPq. A.S.B., D.F.P., S.d'A.S. and M.H.F.B. The authors acknowledge Professor Carlos de Carvalho for computational support at LFTC-DFis-UFPR and at LCPAD-UFPR. M.H.F.B. acknowledges CENAPAD-SP for computational support. G.G. acknowledges partial financial support from the Spanish Ministerio de Economia y Competitividad (Project No. FIS2012-31230). This work was also supported by the Radiation Biology and Biophysics Doctoral Training Programme (RaBBiT, PD/00193/2010) and Grant No. UID/Multi/04378/2013 (UCIBIO).

[1] M. J. Molina and F. S. Rowland, Nature (London) **249**, 810 (1974).
[2] F. S. Rowland and J. Molina, Rev. Geophys. **13**, 1 (1975).
[3] S. M. Schauffler, L. E. Heidt, W. H. Pollock, T. M. Gilpin, J. F. Vedder, S. Solomon, R. A. Lueb, and E. L. Arias, Geophys. Res. Lett. **20**, 2567 (1993).
[4] Z. A. Allah, J. C. Whitehead, and P. Martin, Environ. Sci. Technol. **48**, 558 (2014).
[5] J. A. Ayala, W. E. Wentworth, and E. C. M. Chen, J. Phys. Chem. **85**, 3989 (1981).
[6] S. J. Burns, J. M. Matthews, and D. L. McFadden, J. Phys. Chem. **100**, 19436 (1996).
[7] G. A. Gallup and I. I. Fabrikant, J. Chem. Phys. **135**, 134316 (2011).
[8] T. M. Miller, J. F. Friedman, L. C. Schaffer, and A. A. Viggiano, J. Chem. Phys. **131**, 084302 (2009).
[9] L. A. Pinnaduwage, C. Tav, D. L. McCorkle, and W. X. Ding, J. Chem. Phys. **110**, 9011 (1999).
[10] H.-U. Scheunemann, E. Illenberger, and H. Baumgärtel, Ber. Bunsenges. Phys. Chem. **84**, 580 (1980).
[11] I. Szamrej, W. Tchorzewska, H. Kość, and M. Foryś, Radiat. Phys. Chem. **47**, 269 (1996).
[12] H.-X. Wan, J. H. Moore, and J. A. Tassell, J. Chem. Phys. **94**, 1868 (1991).
[13] M. Bart, P. W. Harland, J. E. Hudson, and C. Vallance, Phys. Chem. Chem. Phys. **3**, 800 (2001).
[14] J. E. Hudson, C. Vallance, M. Bart, and P. W Harland, J. Phys. B: At. Mol. Opt. Phys. **34**, 3025 (2001).
[15] R. Naghma, D. Gupta, B. Goswami, and B. Antony, Int. J. Mass Spectrom. **360**, 39 (2014).
[16] G. P. Karwasz, R. S. Brusa, A. Piazza, and A. Zecca, Phys. Rev. A **59**, 1341 (1999).
[17] R. Naghma, D. Gupta, and B. Antony, J. Electron Spectrosc. Relat. Phenom. **193**, 48 (2014).
[18] A. P. P. Natalense, M. H. F. Bettega, L. G. Ferreira, and M. A. P. Lima, Phys. Rev. A **59**, 879 (1999).
[19] F. Motte-Tollet, M.-J. Hubin-Franskin, and J. E. Collin, J. Chem. Phys. **97**, 7314 (1992).
[20] D. F. Pastega, E. Lange, J. Ameixa, A. S. Barbosa, F. Blanco, G. García, M. H. F. Bettega, P. Limão-Vieira, and F. Ferreira da Silva, Phys. Rev. A **93**, 032708 (2016).
[21] A. S. Barbosa, M. T. do N. Varella, S. d'A. Sanchez, J. Ameixa, F. Blanco, G. García, P. Limão-Vieira, F. Ferreira da Silva, and M. H. F. Bettega, J. Chem. Phys. **145**, 084311 (2016).
[22] K. Takatsuka and V. McKoy, Phys. Rev. A **24**, 2473 (1981).
[23] K. Takatsuka and V. McKoy, Phys. Rev. A **30**, 1734 (1984).
[24] M. H. F. Bettega, L. G. Ferreira, and M. A. P. Lima, Phys. Rev. A **47**, 1111 (1993).
[25] R. F. da Costa, M. T. do N. Varella, M. H. F. Bettega, and M. A. P. Lima, Eur. Phys. J. D **69**, 159 (2015).
[26] See http://cccbdb.nist.gov/ for the value of the polarizability of CH_2Cl_2.
[27] G. B. Bachelet, D. R. Hamann, and M. Schlüter, Phys. Rev. B **26**, 4199 (1982).
[28] M. H. F. Bettega, A. P. P. Natalense, M. A. P. Lima, and L. G. Ferreira, Int. J. Quantum Chem. **60**, 821 (1996).
[29] T. H. Dunning, Jr., J. Chem. Phys. **53**, 2823 (1970).
[30] C. W. Bauschlicher, J. Chem. Phys. **72**, 880 (1980).
[31] E. M. de Oliveira, M. T. do N. Varella, M. H. F. Bettega, and M. A. P. Lima, Eur. Phys. J. D **68**, 65 (2014).
[32] F. Blanco and G. García, J. Phys. B: At., Mol. Opt. Phys. **42**, 145203 (2009).
[33] F. Blanco and G. García, Phys. Lett. A **330**, 230 (2004).
[34] F. Blanco and G. García, Chem. Phys. Lett. **635**, 321 (2015).
[35] D. B. Jones, P. Limão-Vieira, M. Mendes, N. C. Jones, S. V. Hoffmann, R. F. da Costa, M. T. do N. Varella, M. H. F. Bettega, F. Blanco, G. García, O. Ingólfsson, M. A. P. Lima, and M. J. Brunger, J. Chem. Phys. **146**, 184303 (2017).
[37] R. F. da Costa, E. M. de Oliveira, M. H. F. Bettega, M. T. do N. Varella, D. B. Jones, M. J. Brunger, F. Blanco, R. Colmenares, P. Limão-Vieira, G. García, and M. A. P. Lima, J. Chem. Phys. **142**, 104304 (2015).
[36] M. Polasek, M. Jurek, M. Ingr, P. Carsky, and J. Horacek, Phys. Rev. A **61**, 032701 (2000).
[38] R. F. da Costa, M. H. F. Bettega, Márcio T. do N. Varella, E. M. de Oliveira, and M. A. P. Lima, Phys. Rev. A **90**, 052707 (2014).
[39] P. Burrow, A. Modelli, N. S. Chiu, and K. D. Jordan, J. Chem. Phys. **772699** (1982).
[40] K. Aflatooni, G. A. Gallup, and P. D. Burrow, J. Chem. Phys. **132**, 094306 (2010).
[41] F. Blanco, F. Ferreira da Silva, P. Limão-Vieira, and G. García, Plasmas Sources Sci. Technol. **26**, 085004 (2017).
[42] M. Inokuti, Rev. Mod. Phys. **43**, 297 (1971).